J. Fluid Mech. (1975), *vol.* 68, *part* 3, *pp.* 577–590
Printed in Great Britain

The development of turbulence structure in a uniform shear flow

By P. J. MULHEARN† AND R. E. LUXTON‡
Department of Mechanical Engineering, University of Sydney

(Received 24 September 1972 and in revised form 20 February 1974)

Measurements of the streamwise development of a variety of velocity correlations in a uniform shear flow are given and discussed. It is concluded that, in the region in which the Reynolds stresses are approximately constant, the turbulence structure is practically independent of all the initial conditions except the initial length scale. It appears that the preferential amplification of some eddy structures by the mean shear effectively destroys information about the initial conditions, apart from the initial length scale, after a total strain of about 1·5.

1. Introduction

Experimental turbulence research mostly involves the pursuit of limited aims associated with the understanding of particular phenomena. The approach can be via the study of 'naturally occurring' turbulent flows such as wakes, jets and boundary layers, or by the synthesis of much simpler turbulent flow fields which exhibit only some of the features of naturally occurring turbulent flows. The work described in this paper falls into the latter category. The decay of pseudo-isotropic turbulence behind a grid and the subjection of this turbulence to a plane strain (see, for example, Townsend 1956; Tucker & Reynolds 1968; Marechal 1967, 1968) are related problems which have contributed much to our present ideas about turbulence in general. The pseudo-homogeneous uniformly sheared turbulence studied by Rose (1966, 1970), Champagne, Harris & Corrsin (1970), Hwang (1971) and the present writers (1970) is one stage closer to a 'naturally occurring' turbulent shear flow as it involves both plane strain *and* rotation. The above simplified flows can also be studied theoretically with less resort to empiricism than can naturally occurring flows, and it is from the combined theoretical and experimental studies that we derive greatest understanding.

In the present paper we are concerned with the development of quasi-equilibrium turbulence structure from the initial conditions imposed by the device generating the shear flow. The developing structure is pictured through various velocity correlation functions in space–time. Initially the structure is strongly anisotropic and quite different from the initial structures in the studies

† Present address: Division of Environmental Mechanics, C.S.I.R.O., Canberra, A.C.T.
‡ Present address: Department of Mechanical Engineering, University of Adelaide, South Australia 5001.

by Champagne *et al.* (1970) and Hwang (1971), yet in the region downstream in which the Reynolds stresses become constant the structures found in all experiments are remarkably similar, differing only in length scales, which seem to depend on the length scale of the shear-generating device (see § 4). Thus it appears that the mean shear acts preferentially on certain eddies to produce a particular turbulence structure downstream. Once this particular structure has been achieved the details of the initial conditions become of minor importance apart from setting the length scale. This view is similar to that taken by Townsend (1970) when calculating the development of correlation functions in turbulent shear flows.

2. Experimental apparatus

Experiments were performed in an open-return blower wind tunnel driven by a variable-speed motor and centrifugal fan. The working section of the tunnel for the present experiments was 1·5 ft high, 1·0 ft wide and 10 ft long. The roof of the working section was adjusted to give a zero pressure gradient. The actual length of the working section was extended greatly by a simple modification of the two-dimensional diffuser to give a zero pressure gradient, but the small cross-section combined with the low tunnel mean velocity (15 ft s^{-1}) led to thick side-wall boundary layers which certainly influenced measurements downstream of 16 ft and possibly influenced measurements from 10 ft onwards. [For this reason conclusions regarding the behaviour of turbulence at large total strains given in Mulhearn & Luxton (1970) should be regarded as tentative until further experiments are done in a larger wind tunnel.]

The shear flow was generated by means of a non-uniform planar grid of $\frac{1}{8}$ in. steel bars of square cross-section clamped into a drawer which could be slid horizontally into a slot at the outlet from the contraction. A uniform honeycomb 9 in. deep with $\frac{1}{4}$ in. hexagonal cells was placed 2·5 ft downstream from the non-uniform grid to impose a uniform length scale on the flow. The penalty for this was a reduction in the velocity gradient. The working section proper began at the downstream face of the honeycomb (figure 1). Considerable difficulty was experienced in obtaining transverse homogeneity in the turbulence at strain rates greater than about 6 s^{-1}. The large blockage of the honeycomb (approximately one dynamic head) also led to inhomogeneities at mean velocities greater than 20 ft/s. As a consequence the results presented in this paper were obtained with a centre-line velocity of 15 ft/s and a mean strain rate of 5·45 s^{-1}.

Standard DISA hot-wire probes were used with a four-channel constant-temperature anemometer system (Fraser 1972) for mean flow and turbulence measurements. Signals were low-pass filtered at 1 kHz, multiplexed, converted to digital form and stored on magnetic tape for subsequent reduction by a KDF 9 computer in the Basser Computing Laboratory of the University of Sydney. Full details of the data system may be found in Luxton, Swenson & Chadwick (1967) and Fraser (1972)

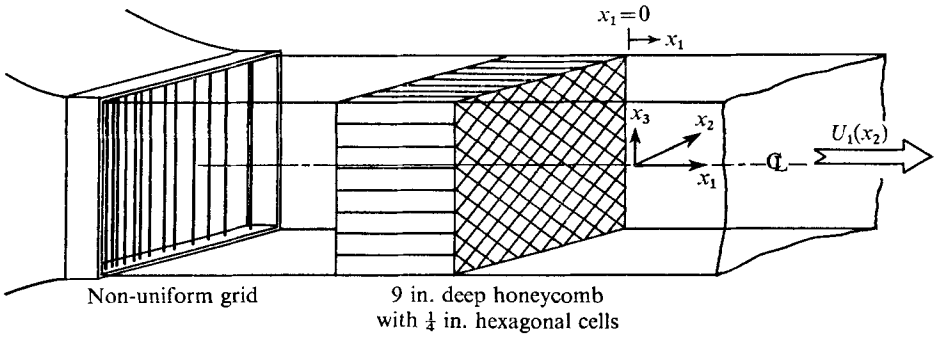

FIGURE 1. Configuration of shear-flow generator, showing bars with non-uniform spacing and honeycomb section. Co-ordinates, x_1, x_2, x_3; mean velocity components,

$$U_1 = U_{\mathbb{Q}} + x_2 dU_1/dx_2, \quad U_2 = U_3 = 0;$$

r.m.s. fluctuating velocity components, u_1', u_2', u_3'.

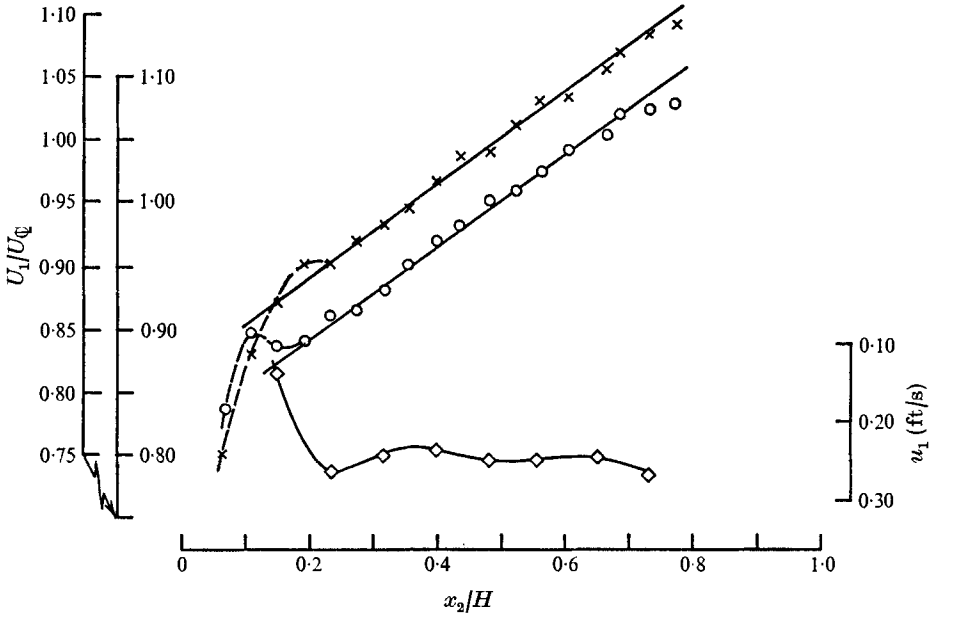

FIGURE 2. Mean velocity profiles at two downstream stations and a typical u_1' profile. ○, $U_1/U_{\mathbb{Q}}$ at $x_1/H = 3{\cdot}3$; ×, $U_1/U_{\mathbb{Q}}$ at $x_1/H = 7{\cdot}54$; ◇, u_1' at $x_1/H = 7{\cdot}54$. H = tunnel width = 1 ft, $x_3/H = 0$ and $dU_1/dx_2 = 5{\cdot}45$ at both stations.

3. The flow field

For at least 10 ft downstream from the honeycomb the mean velocity gradient dU_1/dx_2 in the shear flow remained constant and acceptable homogeneity in the transverse direction was obtained for Reynolds stresses, correlation functions and Taylor microscales. Full results may be found in Mulhearn & Luxton (1970) and distributions of the mean velocity and streamwise r.m.s. velocity fluctuation u' are shown here in figures 2 and 3. The notation is defined in figure 1.

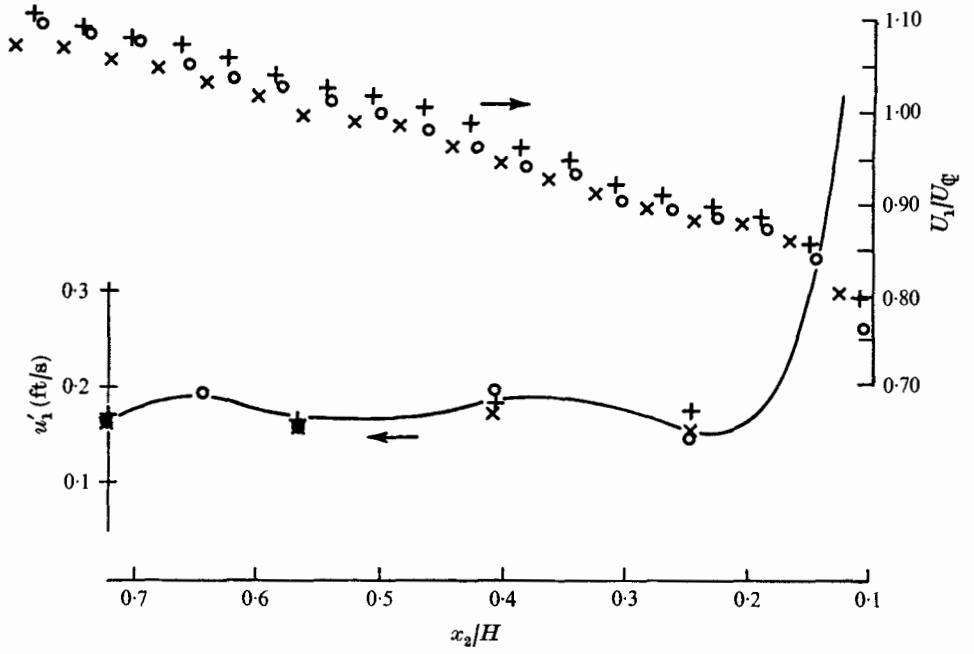

FIGURE 3. Two-dimensionality of mean velocity and u_1' at $x_1/H = 7{\cdot}13$. ○, $x_3/H = -0{\cdot}075$; ×, $x_3/H = -0{\cdot}217$; +, $x_3/H = -0{\cdot}475$.

At $x_1 = 7{\cdot}5$ ft the transverse integral length scale of the flow was approximately one tenth of the width of the region of uniform shear, i.e. that region of the flow in which the mean flow was unaffected by the side-wall boundary layers. The majority of the measurements of space–time correlations reported here were made at or upstream of this station. However, we believe that the flow near the centre-line remained a good approximation to a uniform shear flow of infinite extent up to at least $x_1 = 10$ ft and probably beyond. Given sufficient time, that is, sufficiently far downstream, the turbulence scales must eventually grow until they are constrained by the finite dimensions of the tunnel.

4. Experimental results

The streamwise development of the normal and shear stress fields and of the turbulence length scales is shown in figure 4. At small x_1 the shear stress $-\overline{u_1 u_2}$ is appreciable and the normal stresses $\overline{u_1^2}$, $\overline{u_2^2}$ and $\overline{u_3^2}$ differ significantly from each other, indicating a high degree of anisotropy in the initial conditions at $x_1 = 0$. This differs markedly from the initial conditions in the experiments by Rose (1966), Champagne *et al.* (1970) and Hwang (1971) yet the stress fields in all these experiments including the present ones, when normalized with respect to the total turbulent kinetic energy, tend to become the same downstream.

If the point at which stresses become constant is coincident with the establishment of a quasi-equilibrium in the flow (referred to by Rose (1970) as a 'uniform asymptotic', a concept with which the present writers disagree because of the

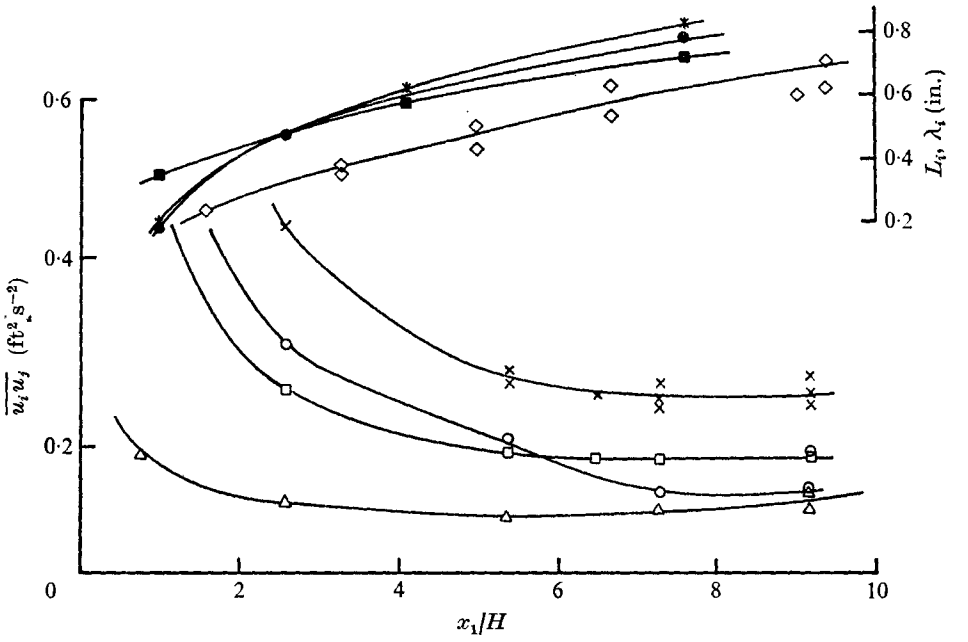

FIGURE 4. Streamwise development of Reynolds stresses and length scales. ×, $\overline{u_1^2}$; ○, $\overline{u_2^2}$; □, $\overline{u_3^2}$; △, $-\overline{u_1 u_2}$; ✳, L_1; ●, L_2; ■, L_3; ◇, λ_{x_1}. $L = \int_0^\infty R_{11}(r_i)dr_i$.

continuous growth of length scales), then it would appear that this state is established more quickly and with a much higher relative turbulence level than was found by Rose (1970) for the $\frac{1}{4}$ in. honeycomb generator studied by Hwang.

Autocorrelations of each of the three fluctuating velocity components at a number of streamwise stations are shown in figure 5. The large negative loop in the $R_{11}(\tau) = \overline{u_1(\mathbf{x}, t)\, u_1(\mathbf{x}, t+\tau)}/\overline{u_1^2(\mathbf{x})}$ autocorrelation at small x_1 again indicates initial anisotropy. At large x_1 this autocorrelation has a similar form to that found by Champagne *et al.* (1970), see their figure 16, but the present results indicate a more pronounced negative loop. The $R_{22}(\tau)$ and $R_{33}(\tau)$ curves closely resemble each other, indicating that their power spectra must likewise be similar as was found by Champagne *et al.* for large x_1.

As x_1 increases the time scales increase as is indicated by the zero-crossing points of the autocorrelations in figure 5. However, the rate of change of shape of the autocorrelations decreases, which suggests the emergence of a preferred turbulence structure.

The time correlations in figure 5 may be regarded as streamwise spatial correlations if we use Taylor's hypothesis to write

$$\tau = -r_1/U_c, \tag{1}$$

where U_c is the convection velocity of the turbulence and r_1 is the spatial separation in the streamwise direction. To justify the use of Taylor's hypothesis the method of Stegen & Van Atta (1970) was used to find the phase velocity as a

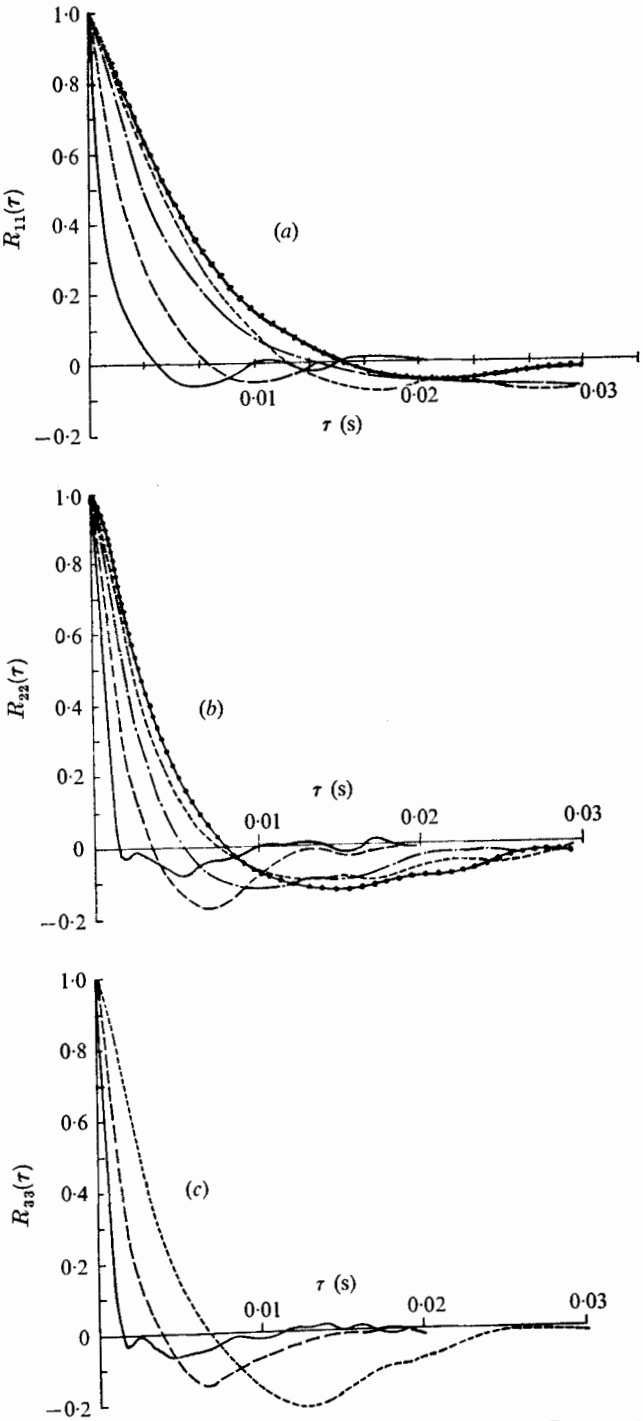

FIGURE 5. Streamwise development of autocorrelations. (*a*) $R_{11}(\tau)$. (*b*) $R_{22}(\tau)$. (*c*) $R_{33}(\tau)$. ——, $x_1/H = 0{\cdot}81$; — —, $x_1/H = 2{\cdot}74$; — · —, $x_1/H = 5{\cdot}4$; ·····, $x_1/H = 7{\cdot}52$; ●—●, $x_1/H = 9{\cdot}2$. $x_2 = x_3 = 0$ throughout.

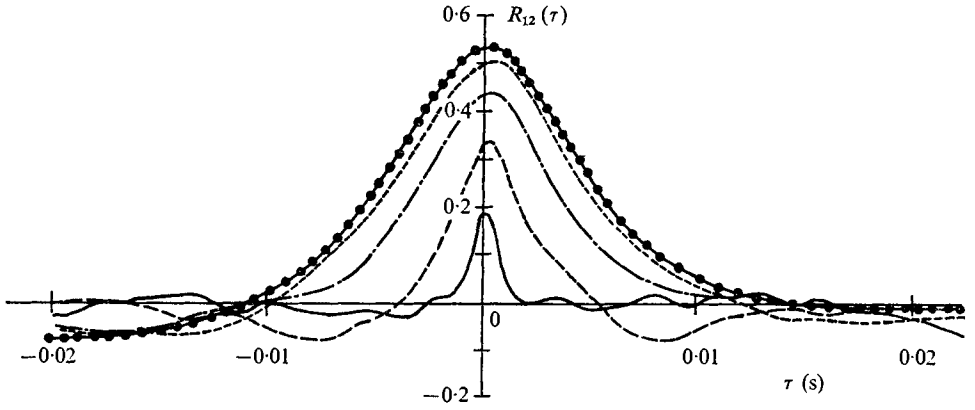

FIGURE 6. Streamwise development of cross-correlation $-R_{12}(\tau)$.
Curves as for figure 5. $x_2 = x_3 = 0$ throughout.

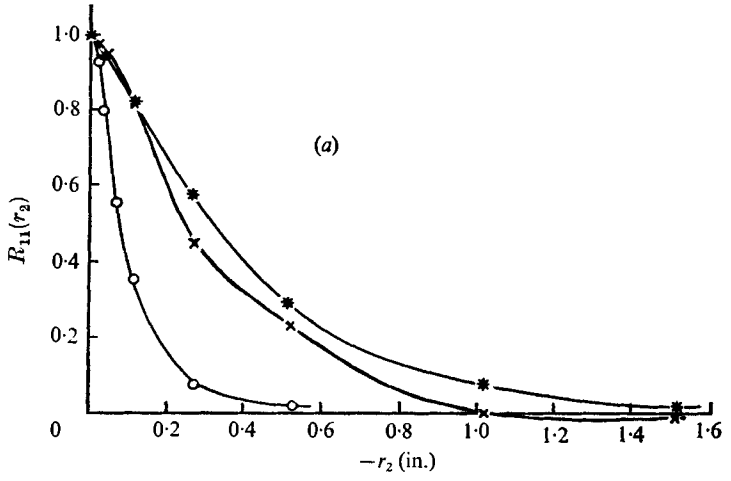

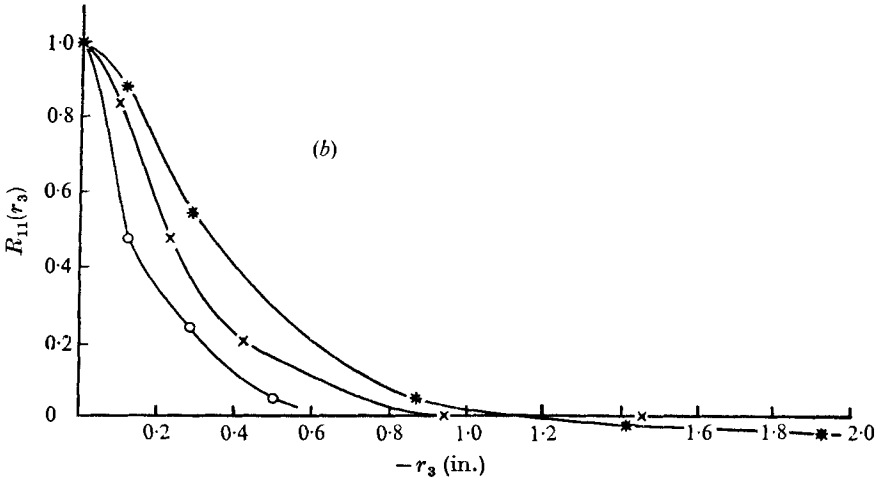

FIGURE 7. Streamwise development of correlations with lateral separation. (*a*) $R_{11}(r_2)$. (*b*) $R_{11}(r_3)$. ○, $x_1/H = 0{\cdot}83$, total strain = 0·3; ×, $x_1/H = 4{\cdot}16$, total strain = 1·5; ✳, $x_1/H = 7{\cdot}5$, total strain = 2·7.

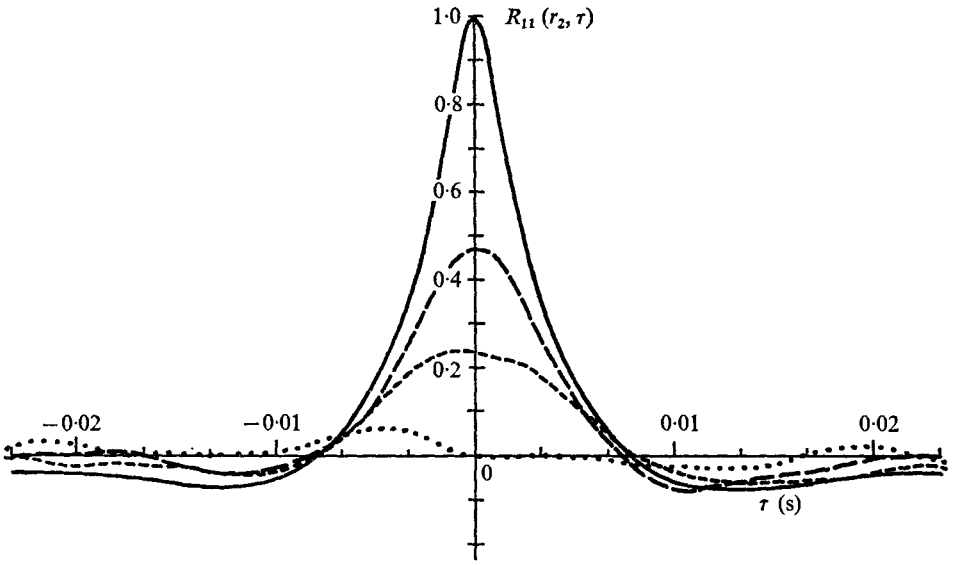

FIGURE 8. Space–time correlation $R_{11}(r_2, \tau)$ at $x_1/H = 4{\cdot}16$. ——, $r_2 = 0$; — — —, $r_2 = 0{\cdot}269$ in.; – – – – –, $r_2 = 0{\cdot}521$ in.; · · · · · · ·, $r_2 = 1{\cdot}020$ in.

function of frequency, and this was found to be constant for all frequencies. Space–time correlation data showed that U_c was equal to the local mean velocity.

As do the autocorrelations, the cross-correlation

$$R_{12}(\tau) = \overline{u_1(\mathbf{x}, t)\, u_2(\mathbf{x}, t+\tau)}/\overline{u_1 u_2(\mathbf{x})},$$

shown in figure 6, indicates a growth in scale with distance downstream but a decrease in the rate of change of correlation shape. This may also be regarded as a streamwise spatial correlation by application of (1).

The correlations between streamwise velocity fluctuations at points distributed transversely across the flow and at zero time delay,

$$R_{11}(r_i) = \overline{u_1(\mathbf{x}, t)\, u_1(\mathbf{x}+r_i, t)}/[\overline{u_1^2(\mathbf{x})}\ \overline{u_1^2(\mathbf{x}+r_i)}]^{\frac{1}{2}},$$

where $i = 2, 3$, are shown in figure 7. Here r_2 is taken as positive up the velocity gradient. At large x_1 the $R_{11}(r_3)$ curve has a negative loop and the $R_{11}(r_2)$ curve remains positive in agreement with the results of Champagne *et al.* (1970) and of Hwang (1971). However, Hwang found that the shapes of the transverse correlations were a function of the initial length scale set by a grid placed downstream of his shear-flow generator. Reduction of the mesh size of the grid from 2 in. to $\frac{1}{2}$ in. (see his figures 19 and 20) caused the $R_{11}(r_2)$ curve to become less 'fat', the value of $-r_3$ at the zero-crossing point of the $R_{11}(r_3)$ correlation to decrease slightly and the negative loop to become smaller. In the present experiments the cell size of the honeycomb was $\frac{1}{4}$ in., and if this is taken to be an equivalent mesh size, the $R_{11}(r_2)$ and $R_{11}(r_3)$ correlations measured at large x_1 agree well with the trend of Hwang's data. From $x_1/H = 0{\cdot}83$ to $4{\cdot}16$ the correlation $R_{11}(r_2)$ changes more rapidly than it does from $x_1/H = 4{\cdot}16$ to $7{\cdot}5$, again suggesting an approach to a preferred state.

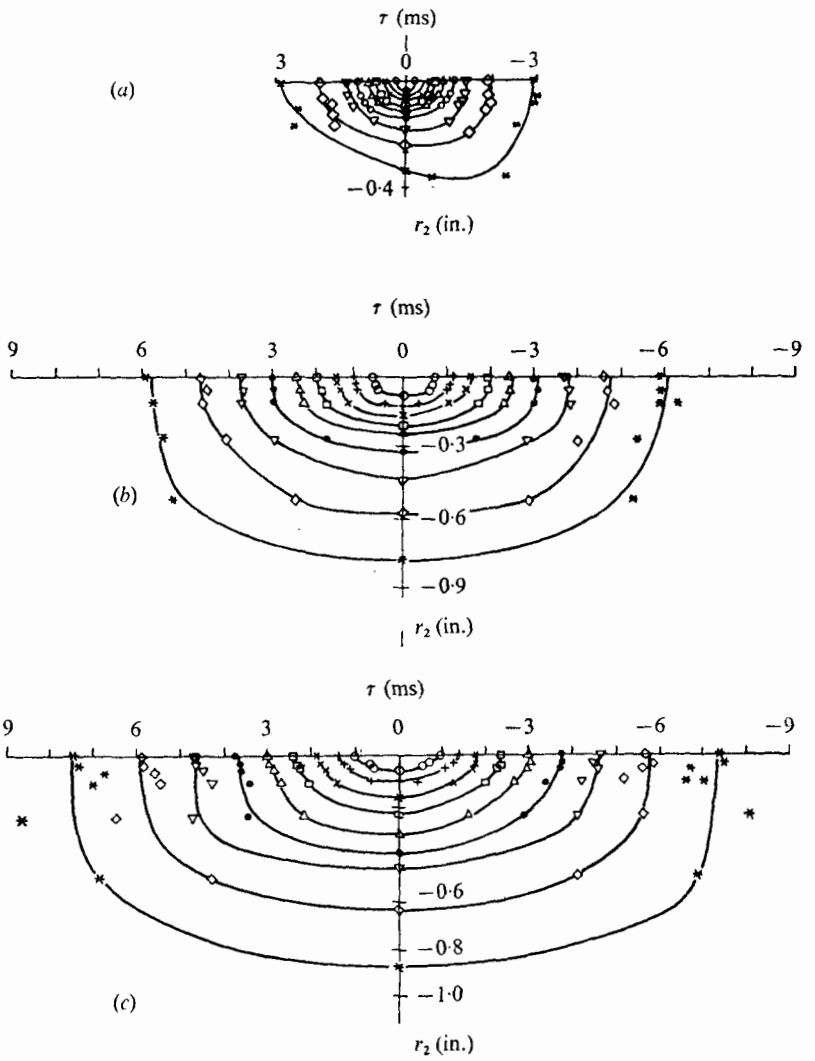

FIGURE 9. Isocorrelation contours for the space–time correlation $R_{11}(r_2, \tau)$. (*a*) $x_1/H = 0{\cdot}83$, total strain = 0·3. (*b*) $x_1/H = 4{\cdot}16$, total strain = 1·5. (*c*) $x_1/H = 7{\cdot}5$, total strain = 2·7. The contours are all drawn to the same scale. $R_{11}(r_2, \tau)$: ○, 0·9; +, 0·8; ×, 0·7; □, 0·6; △, 0·5; ●, 0·4; ▽, 0·3; ◇, 0·2; ✳, 0·1.

From the transverse space–time velocity correlations

$$R_{11}(r_1, \tau) = \overline{u_1(\mathbf{x}, t)\, u_1(\mathbf{x}+r_i, t+\tau)} / [\overline{u_1^2(\mathbf{x})}\, \overline{u_1^2(\mathbf{x}+r_i)}]^{\frac{1}{2}},$$

where $i = 2, 3$, illustrated by the $R_{11}(r_2, \tau)$ curves of figure 8, a set of isocorrelation contours was constructed. These are shown in figures 9 and 10 and have been plotted such that the scale on the τ axis corresponds to an r_1 axis of the same scale as the r_2 and r_3 axes if Taylor's hypothesis is applied with the convection velocity taken as the local streamwise velocity at $\mathbf{r} = 0$. Thus the isocorrelation contours of figures 9 and 10 give a picture of the development of the turbulence

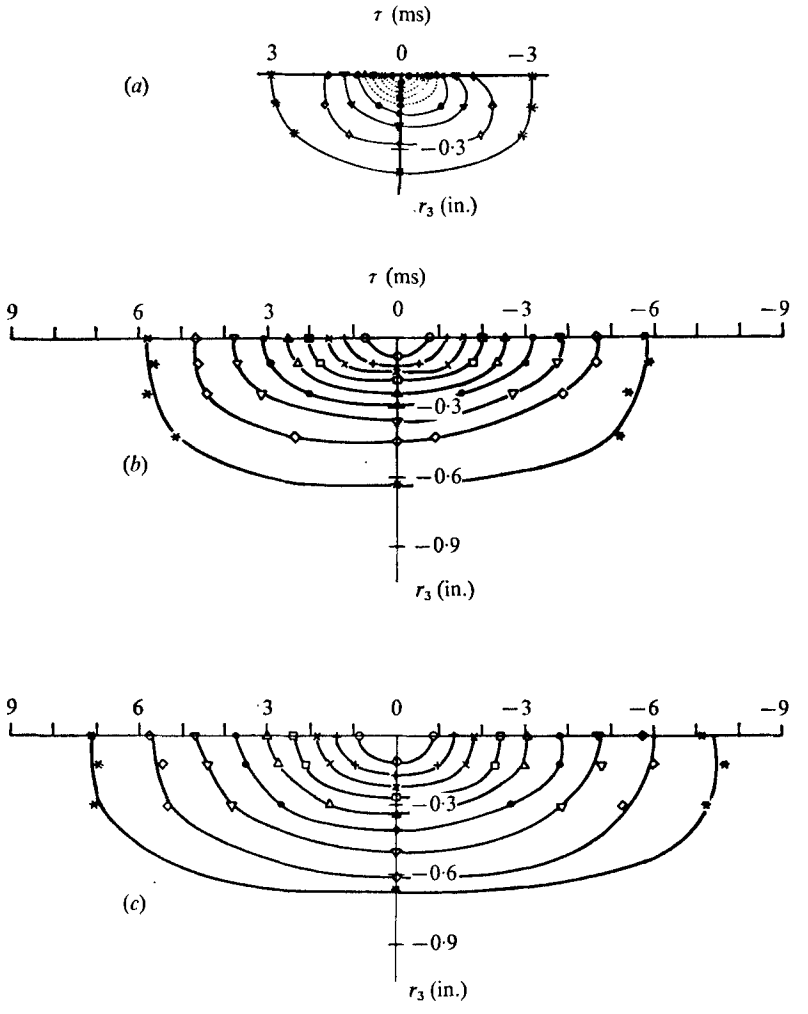

FIGURE 10. Isocorrelation contours for the space–time correlation $R_{11}(r_3, \tau)$. (*a*)–(*c*) and symbols as for figure 9.

structure as it proceeds downstream from its anisotropic initial condition under the influence of the mean shear.

Taking the structure at $x_1 = 0{\cdot}83$ ft, which corresponds to a total strain $x_1 dU_1/U_1 dx_2$ of 0·3, as being indicative of the initial conditions at $x_1 = 0$, we see that the initial asymmetry is largely eliminated by $x_1 = 4{\cdot}16$ ft, i.e. after a total strain of 1·5. Further straining to $x_1 = 7{\cdot}5$ ft (total strain = 2·72) causes predominantly only a change in scale. The scale in the r_2 direction becomes larger than that in the r_3 direction as was found by Champagne *et al.* (1970), but unlike the results shown in their figure 25 for

$$\overline{u_1(\mathbf{x};t)\,u_1(\mathbf{x}+(r_1,r_2,0);t)}/[\overline{u_1^2(\mathbf{x})}\;\overline{u_1^2(\mathbf{x}+(r_1,r_2,0))}]^{\frac{1}{2}}$$

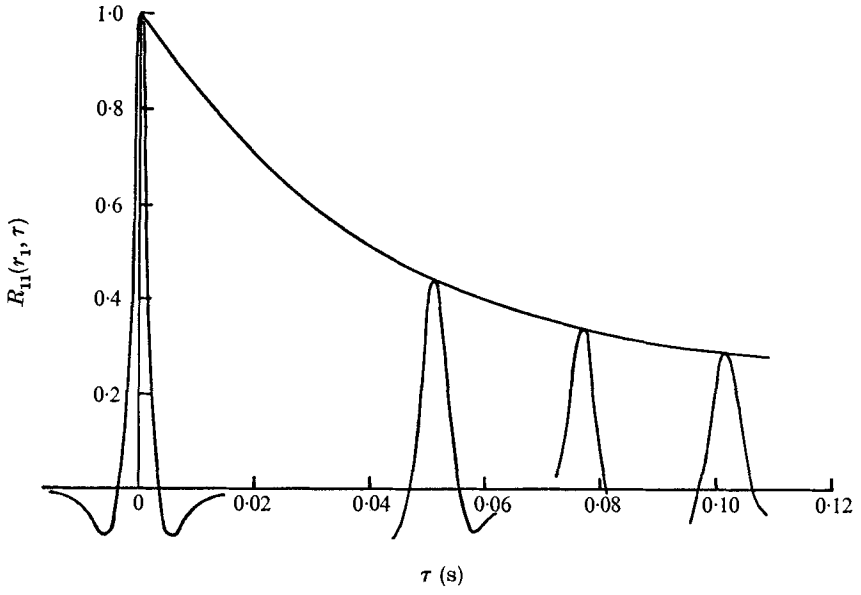

FIGURE 11. Space–time correlation $R_{11}(r_1, \tau)$ at $x_1/H = 0{\cdot}81$.

for large x_1, the present results do not show any marked degree of asymmetry.† The asymmetrical correlation contours in the present experiments occur in a rapidly changing part of the flow. The small asymmetry at downstream stations is of the same sign as that found by Champagne *et al.* as may be seen by comparing the skewness of $R_{11}(r_2, \tau)$ at $x_1/H = 4{\cdot}16$ (figure 8) with their figure 27. Note, however, that the skewness in the present experiments is confined to small τ only, except for $r_2 = 1{\cdot}02$ in., where correlation values are very low. In the experiments of Champagne *et al.* the streamwise rate of change of the length scale was larger than that measured in the present experiments. This may have been due to their larger initial length scale. However, the change in scale over a correlation width does not appear to be sufficient to explain the marked asymmetry of their correlation contours.

Space–time correlations with separations in both the r_1 and r_2 directions were measured at two stations to give further information on the development of scales and on the lifetime of structures. The plot of $R_{11}(r_1, 0, 0; \tau)$ at $x_1 = 0{\cdot}83$ ft shown in figure 11 is typical of these measurements. From them a time delay $\tau = \tau_M$ for optimum correlation can be determined and this can be used in developing isocorrelation contours of $R_{11}(r_1, r_2, 0; \tau_M)$, which give a picture of the eddy structure in a frame of reference moving at the local mean velocity. This is shown in figure 12 for $x_1 = 0{\cdot}81$ and $5{\cdot}4$ ft. It can be seen that the scale in the r_2

† If space correlations are constructed from the time correlations of figure 9 by using a convection velocity $U_c = \frac{1}{2}(\overline{U}(x_2) + \overline{U}(x_2 + r_2))$, the degree of symmetry of the contours is unaffected. They are only very slightly contracted as U_c varies by only about 3 % over the range of r_2. If this extension of Taylor's hypothesis is applied to the space–time correlations of Champagne *et al.* (their figure 27) the agreement with their measured space correlations (their figure 23) is good.

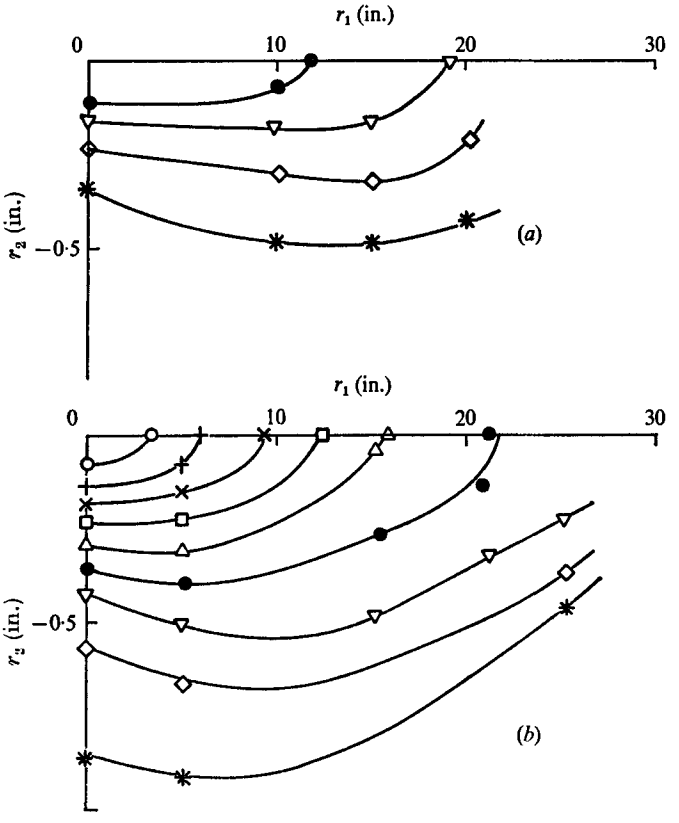

FIGURE 12. Isocorrelation contours for optimum values of the space–time correlation $R_{11}(r_1, r_2, 0; \tau_M)$. (a) $x_1/H = 0{\cdot}81$, total strain = 0·29. (b) $x_1/H = 5{\cdot}4$, total strain = 1·95. Symbols as for figure 9.

direction grows more rapidly than that in the streamwise direction between these two stations. The length scales deduced from these correlations are smaller than those measured by Champagne *et al.* (1970) and this is no doubt due to the larger length scale imposed by their shear-flow generator.

5. Discussion

It has been shown that the initial turbulence structure in the present experimental flow was strongly anisotropic, unlike that in the flows studied by Champagne *et al.* (1970) and Hwang (1971). A further indication of the development from this anisotropic initial condition is given by consideration of the orientation α_σ of the principal axes of the Reynolds stress tensor and the ratio σ_a/σ_b of the principal stresses. These are shown in figure 13. In isotropic turbulence $\alpha_\sigma = \pm 45°$ and $\sigma_a/\sigma_b = 1$. In the present flow the values approach $\alpha_\sigma = +62°$ or $-28°$ and $\sigma_a/\sigma_b = 3{\cdot}4$ at around $x_1/H = 8$, which corresponds to a total strain of 2·9. The values of α_σ are the same as the asymptotic values found by Champagne *et al.* (1970) but indicate an anisotropy slightly greater than that found by

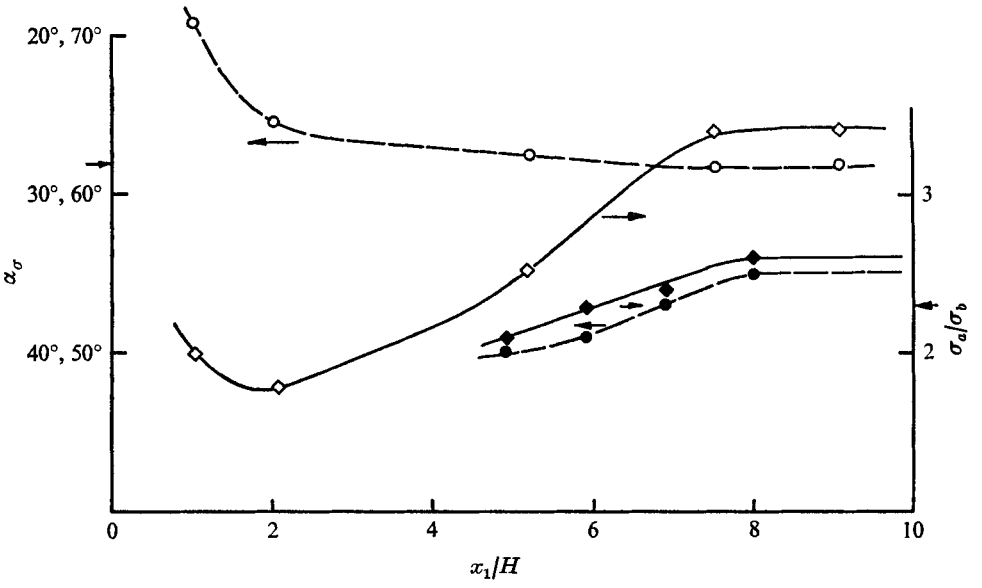

FIGURE 13. Streamwise development of the orientation α_σ of the principal axes of the Reynolds stress tensor and of the ratio σ_a/σ_b of the principal stresses. Closed symbols, Hwang (1971); open symbols, the present data. Arrows on the ordinates are values from Champagne *et al.* (1970) for large x_1/H. ○, ●, α_σ; ◇, ◆, σ_a/σ_b.

Hwang (1971). The principal stress ratio σ_a/σ_b is larger than that found in either of the above investigations and is more typical of the values found in boundary layers and channels.

Although there are some differences in detail between the flow structures found in the quasi-equilibrium region of the present flow and those found by other workers, the major features are remarkably similar in spite of the considerable differences in initial conditions. The most obvious differences arise from differences in the initial length scales set by the shear-generating devices. On this evidence it appears that the mean shear acts to amplify preferred eddy structures, while other structures decay, giving a structure downstream (i.e. after a total strain of about 1·5) which is largely independent of the initial conditions apart from a scale effect. Townsend (1970) assumed this to be true and used only the total strain and an initial length scale L as external parameters when calculating the development of correlation functions in turbulent shear flows. His predicted correlations were normalized with respect to L. Although the present experiments do not fully justify this normalization, they certainly support the spirit of Townsend's analysis.

This investigation forms part of a programme of research at the University of Sydney supported by the Australian Research Grants Committee, the Australian Institute of Nuclear Science and Engineering and the Commonwealth Scientific and Industrial Research Organization.

REFERENCES

CHAMPAGNE, F. H., HARRIS, V. G. & CORRSIN, S. 1970 *J. Fluid Mech.* **41**, 81.

FRASER, D. 1972 Ph.D. thesis, Department of Mechanical Engineering, University of Sydney.

HWANG, W. S. 1971 Ph.D. thesis, School of Engineering and Applied Science, University of Virginia.

LUXTON, R. E., SWENSON, G. G. & CHADWICK, B. S. 1967 *The Collection and Processing of Field Data* (ed. E. F. Bradley & O. T. Denmead), pp. 497–509. Interscience.

MARECHAL, J. 1967 *C.r. hebd. Séanc. Acad. Sci., Paris*, A **265**, 69, 478.

MARECHAL, J. 1968 *C.r. hebd. Séanc. Acad. Sci., Paris*, A **267**, 364.

MULHEARN, P. J. & LUXTON, R. E. 1970 *Chas. Kolling Res. Lab., University of Sydney, Rep.* TNF-19.

ROSE, W. G. 1966 *J. Fluid Mech.* **25**, 97.

ROSE, W. G. 1970 *J. Fluid Mech.* **44**, 767.

STEGEN, G. R. & VAN ATTA, C. W. 1970 *J. Fluid Mech.* **42**, 689.

TOWNSEND, A. A. 1956 *The Structure of Turbulent Shear Flow.* Cambridge University Press.

TOWNSEND, A. A. 1970 *J. Fluid Mech.* **41**, 13.

TUCKER, H. J. & REYNOLDS, A. J. 1968 *J. Fluid Mech.* **32**, 657.